

# Nonlinear modeling of Pancake DC Limited Angle Torque Motor based on LuGre friction model

F. S. Ahmed\*, S. Laghrouche, M. El Bagdouri

Laboratoire Systèmes et Transports, Université de Technologie de Belfort-Montbéliard,  
90000 Belfort, France

\*fayez-shakil.ahmed@utbm.fr

**Abstract** -This paper addresses the physical modeling and identification of Torque Motor based mechatronic actuators used in the air path of the engine of a Drive-by-Wire automobile. The torque motor has non-linear torque characteristics with respect to the rotor position due to its mechanical construction. A study based on two Pancake DC Torque motors has been carried out with two motors of different stator construction. A physical model has been proposed and its parameters have been identified for the two motors. Special attention has been paid on modeling nonlinearities due to torque characteristics and friction. LuGre friction model has been used to incorporate friction nonlinearities. Comparison between simulation and experimental results shows the effectiveness of the proposed model.

**Index terms** — Torque Motor, Mechatronic Actuator; Modeling; Drive-by-Wire; Air Path; LuGre; Automotive Control

## I. INTRODUCTION

In modern automobile Drive-by-Wire (DbW) systems with mechatronic actuators [1, 2], the modeling of nonlinearities is of extreme importance [3]. Such actuators have to be small enough, so as not to hinder in the over all engine design [4], which leads to problems of miniaturization. Also, mechatronic actuators are prone to mechanical non-linearities, such as gearbox friction and backlash and stick slip and load perturbations [5, 6, 7].

Direct Drive motors, such as the Limited Angle Torque Motor have been in use for a long time in the aerospace industry [7, 8, 9]. These motors provide limited angular motion, suitable for actuator purposes, at a relatively high torque. They can hence be coupled to the mechanical part of the actuator without any additional parts or reduction [7, 9]. This leads to better tracking and positioning control of actuators since the nonlinearities associated with gears are no longer present [8]. Their improved size-to-torque ratio and fast response time are also an asset for the designer [8]. With a torsion spring, it can be used efficiently and effectively for continuous position actuators [10]. Unfortunately, not much literature is present on this motor.

Effective control strategy for the torque motor demands a comprehensive physical model which takes the system nonlinearities into consideration [3].

These nonlinearities are mainly due to friction and spring pre-compression [11]. In this paper, we have proposed such a model. This model is based on the physical parameterization of the motor-spring system dynamics as a second order system. Friction and its associated phenomena have been incorporated using the LuGre friction model. This model is the most comprehensive friction model [12], i.e. it can effectively model multiple nonlinear phenomena that are associated with friction, such as Stribeck effect and stick-slip [12, 13].

Two actuators have been taken under study, both related to the automobile engine air path. Both these actuators use torque motors. The first is a ‘Double Air Mixer’, an apparatus to bypass the exchanger. This actuator consists of two butterfly valves that are controlled using separate, identical torque motors. The torque motors for this application are manufactured by Delphi®. The second actuator that we have found using torque motor is the Valeo Exhaust Gas Recirculation actuator. This consists of a linear valve with a torque motor and a cam for rotary-to-linear motion conversion.

This paper is organized in the following manner. Section 2 deals with overview of the torque motor and its application in the above mentioned actuators. In section 3, a mathematical model is proposed for the torque motor as a motor-spring system. In section 4 friction and its modeling have been discussed, with special emphasis on the LuGre model. Section 5 presents the complete state space representation of the model. The parameters of the motors used in the two actuators have been identified in section 6. The model has been validated through comparison between simulation and experimental results. Some conclusions have been presented in section 8.

## II. THE PANCAKE TORQUE MOTOR

A torque motor consists of a rotor and stator assembly. A permanent magnet divided into a series of North-South (N-S) equal surface alternations is fixed to the rotor. The rotor can be seen in fig. 2. Ferromagnetic cores on the stator surrounded by coils make up another series of S-N or N-S alternations according to the current polarity in the coils. In the

angular range between magnet poles, the magnetic interaction produces a torque where the direction depends on the polarity of the current. The detent torque is negligible on the stroke [10].

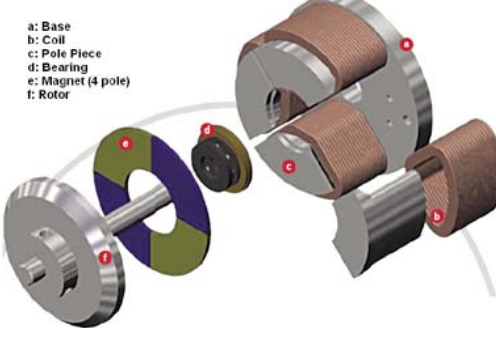


Figure 1: Torque Motor Stator Design (1 Coil per Pole Piece)

a- base, b- coil, c- pole piece (courtesy Sonceboz)

The motor works by attracting the permanent magnet on the rotor to the alternately polarized stator poles. This limits the working angle of the motor; for a four pole piece motor, the rotor can move only 90°. Also, the rotor would not move if the permanent magnet poles are aligned with the pole piece. Therefore the effective rotation, the typical stroke of a system with four alternations is around 70° [4].

The rotor is constructed with an axial shaft and an iron plate pressed to it. The plate is then embedded with the disk shaped permanent magnet. The rotor is same in all torque motors of such constructions, however two different stator constructions are known. The first, used by Delphi, consists of four separate pole pieces (fig. 1), each wound with its own coil. Thus the magnetic polarity is developed by alternate energizing of each coil. The second construction, used by Valeo, involves a single coil wound around a large pole piece. The face of this large pole piece is divided into two to obtain two separate poles of the same polarity. The other two poles of the opposite polarity are formed by separate pole pieces which are connected to the central pole piece through a metallic plate (fig. 2).

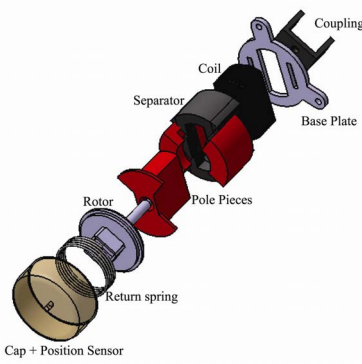


Figure 2: Valeo Torque Motor (Variation: Single coil stator design)

Fig. 3 shows the typical torque characteristics of a torque motor. It can be seen that the torque is not

constant for a constant current, but a function of the angle as well. The torque weakens as the rotor magnets align with the stator poles. Due to this, a linear relationship between the motor power supply and angle can not be found throughout the operating range of the motor.

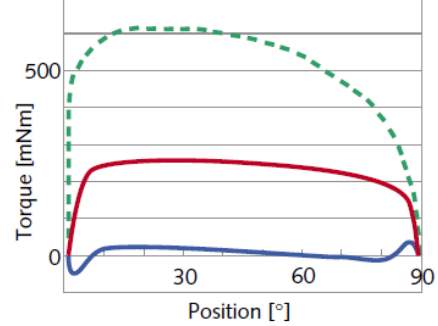


Figure 3: Torque Motor Characteristics w.r.t. Angle (courtesy Sonceboz)

In the case of a torque motor, the spring plays a very important role since without the spring, the motor can have only two stable states and the rotor aligns itself to the stator as soon as power is applied to the stator coils. The advantages of this type of motor are:

- Good torque/size and torque/mass ratio
- Very rapid response due to low rotor inertia (no windings)
- The rotor magnet being the only expensive part
- Direct drive due to high torque (no gear reduction required)

### III. MODELING

The system was modeled as the relationship between the input voltage and the output shaft angle, including motor and spring dynamics and friction. As can be seen in fig. 5, the system does not follow the same path in both directions, in terms of voltage and angle. The hysteresis between these two paths is due to the presence of friction. Friction is the force that opposes the relative motion between two bodies in contact. Another factor prominent in fig. 5 is the slight nonlinearity between input and output in the Valeo curve. As mentioned earlier that the torque produced in the motor varies with the rotor angular position. Therefore we see that the system gain decreases as the motor approaches its end point.

The electromagnetic torque of a torque motor, as we have mentioned before, is a function of the rotor position, and depends upon the rate of change of magnetic flux linkage with respect to position:

$$T_m = K_a(\theta)i_a$$

Where

$$K_a(\theta) = \frac{d\phi(i, \theta)}{d(\theta)}$$

Where  $\phi(i, \theta)$  represents the flux linkage between the stator and rotor. For simplification purposes, we shall assume that the flux is linear with respect to current.

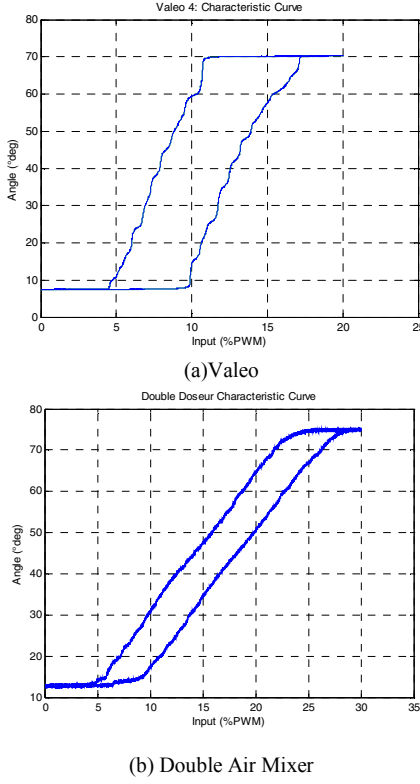


Figure 5: Characteristic Curves (Experimental)

The system dynamics can be represented by the following electrical and mechanical equations:

$$V_a = i_a R_a + L_a \frac{di_a}{dt} + E_a \quad (1)$$

$$T_m = T_s + T_{pc} + T_f + J_{tot} \frac{d\omega}{dt} \quad (2)$$

In equation (1),  $V_a$  is the armature voltage,  $i_a$  is the armature current,  $R_a$  is the motor coil resistance,  $L_a$  is the motor coil inductance.  $E_a$  is the motor back EMF and is defined as:

$$E_a = K_a(\theta)\omega \quad (3)$$

Where, and  $\omega$  is the angular velocity of the motor shaft. In simulation,  $K_a(\theta)$  can be implemented through interpolation of experimental values of torque measured at different angles. In equation (2),  $J_{tot}$  is the total moment of inertia of the system.  $T_m$  is the electromagnetic torque, which, from the reference of the output shaft, can be expressed as:

$$T_m = K_a(\theta)i_a \quad (4)$$

$T_s$ , the spring torque can be defined by:

$$T_s = K_{spr}\theta \quad (5)$$

$T_f$  is the friction force, the static friction is considered here.  $T_{pc}$  is the spring pre-compression torque working against the motor before it starts to move. Replacing (3), (4) and (5) in equations (1) and (2):

$$K_a(\theta)i_a = J_{tot} \frac{d\omega}{dt} + K_{spr}\theta + T_{pc} + T_f \quad (6)$$

As in general, the transitory current can be neglected since the mechanical time constant is generally much greater than the electrical time constant [11]. From equation (3),  $E_a$  can be replaced in equation (1). Replacing equation (1) in equation (6), the motor dynamics can then be represented by the second order system with a second member:

$$\frac{K_a(\theta)V_a}{R_a} = J_{tot} \frac{d^2\theta}{dt^2} + \frac{K_a^2(\theta)}{R_a} \frac{d\theta}{dt} + K_{spr}\theta + (T_{pc} + T_f) \quad (7)$$

The friction force,  $T_f$  is modeled in the next section, while the pre-compression,  $T_{pc}$  is constant and must be overcome by the motor before the shaft starts to move. Let the following variable change:

$$\bar{V}_a = V_a - V_a^* \quad \text{Where } V_a^* = \frac{T_f R_a}{K_a} + \frac{T_{pc} R_a}{K_a}$$

Where  $V_a^*$  is defined as the voltage required to overcome  $T_{pc}$  and  $T_f$ . Then, replacing  $V_a$  in equation (7), the system dynamics become:

$$\frac{K_a(\theta)\bar{V}_a}{J_{tot}R_a} = \frac{d^2\theta}{dt^2} + \frac{K_a^2(\theta)}{R_a J_{tot}} \frac{d\theta}{dt} + \frac{K_{spr}}{J_{tot}} \theta$$

Considering initial conditions to be zero, the Laplace transform and the transfer function of the system comes out to be:

$$\frac{\theta(s)}{\bar{V}_a(s)} = \frac{\frac{K_a(\theta)}{J_{tot}R_a}}{s^2 + \frac{K_a^2(\theta)}{R_a J_{tot}} s + \frac{K_{spr}}{J_{tot}}} \quad (8)$$

This transfer function can be compared to the general form of a second order system,

$$\frac{Y(s)}{X(s)} = \frac{K\omega_n^2}{s^2 + 2\zeta\omega_n s + \omega_n^2}$$

Where

$$\omega_n = \sqrt{\frac{K_{spr}}{J_{tot}}}, \zeta = \frac{K_a^2(\theta)}{2R_a\sqrt{J_{tot}K_{spr}}}, K = \frac{K_a(\theta)}{K_{spr}R_a}$$

#### IV. FRICTION

The hysteresis seen in the characteristic curves of fig. 5 is due to friction [3, 7, 11]. Friction can be divided into two components. The first is the static part  $T_s$ , which is has to be overcome to start the relative motion between two surfaces [11, 12]. It arises due to irregularities in the surfaces in contact. At rest, lubrication is not effective and the surfaces slide over each other, offering more resistance. A body can move only if it has a force greater than  $T_{s\_max}$ .

The second component, dynamic friction also comprises of two further components, Coulomb and Viscous friction. Coulomb friction  $T_c$  is the minimum value to which friction can go to while the object moves, it depends upon the materials in contact. Normally, the values static and coulomb frictions are

close. The viscous friction [12] is a function of velocity and is defined as a coefficient of viscous friction,  $X_v$  multiplied by the velocity  $\omega$  of the system. Viscous friction is due to lubricants. Dynamic friction can hence be written as [12]:

$$T_v = \text{sgn}(\omega) [X_v \cdot \text{abs}(\omega) + T_c]$$

When a body starts from zero velocity, i.e. breaks away from static friction, the transition between static friction (or break-away force) and dynamic friction is called Stribeck effect [12, 13]. These effects can be understood better through fig. 6.

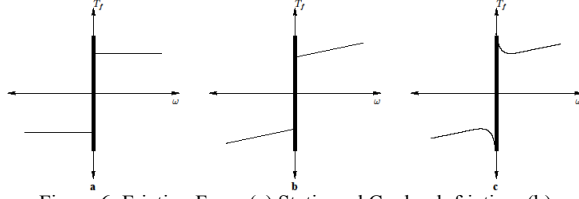


Figure 6: Friction Force (a) Static and Coulomb friction, (b) Viscous friction added, (C) Stribeck effect

#### A. Friction modeling

The actual causes of different phenomena related to friction are very difficult to characterize since they depend upon a large variety of physical phenomena [12, 15]. Therefore different people have modeled the effects of friction in different manners. The available models can be divided into static and dynamic models. It is important to remember that the static friction model is not the same as static friction itself. The model is called static because it does not take the dynamic frictional phenomena into account.

Static friction models do not solve the problem of discontinuity in simulation [12, 14]. Instead, static friction is modeled using other means, such as countering the input torque using a saturated version of the input torque. Dynamic models have a dynamic response to the velocity of the system. Hence they are non-linear but continuous models, more effective in simulation. Dynamic friction models tend to be rate dependent, i.e. their response is different for different frequencies (rate of change of input velocity). The simplest of dynamic friction models is the Dahl Model [12] which models coulomb and viscous frictions by considering the irregularities or asperities of the surfaces in contact, as springs. When a tangential force is applied, the springs stretch, until they reach their elastic limit and ‘break’. This model takes the following form:

$$\begin{aligned} T_f &= \sigma_o z \\ \dot{z} &= \omega - \frac{\sigma_o |\omega|}{T_c} z \end{aligned}$$

Where  $z$  is the average deflection of the springs before breaking and  $\sigma_o$  is their stiffness coefficient. In practice,  $\sigma_o$  defines the slope of the static friction line and the magnitude of the static friction is taken equal to coulomb friction,  $T_c$ . The Dahl model provides a good dynamic strategy for friction modeling; it however does not take into account the stick-slip phenomenon or the Stribeck effect [12].

#### B. LuGre Friction Model

The LuGre Friction model is an extension of the Dahl model [12]. It models asperities as elastic bristles instead of springs. Motion, according to this model occurs when the bristles start ‘slipping’. It allows for the static friction to be modeled separately, and also incorporates Stribeck effect in the model [12, 13, 15, 17]. Hence it can be used to model a greater number of phenomena as compared to the Dahl model [16, 18]. For example, the difference between static and coulomb friction magnitudes can be used in modeling the so-called Stick Slip motion [13, 16, 18]. The LuGre model has the following form:

$$\left. \begin{aligned} T_f &= \sigma_o z + \sigma_1 \dot{z} + \sigma_2 \omega \\ \dot{z} &= \omega - \sigma_o \frac{|\omega|}{g(\omega)} z \end{aligned} \right\} \quad (9)$$

Again,  $z$  is the average deflection of the springs.  $T_f$  is the friction force and  $\sigma_o$  is the stiffness coefficient, modeling the static friction part.  $\sigma_1$  is the damping coefficient which stabilizes the dynamics in the Stribeck region. It is related with the micro displacement of the bristles [18].  $\sigma_2$  is the coefficient of viscous friction. The most important difference between the Dahl and LuGre model is the introduction of  $g(\omega)$ . This function models the Stribeck effect as a function of velocity. If  $\omega$  is the velocity at which Stribeck effect takes place (Stribeck velocity), then  $g(\omega)$  can be expressed as:

$$g(\omega) = T_c + (T_s - T_c) e^{(-\omega/|\omega_s|)^\alpha} \quad (10)$$

$\alpha$  defines the shape of the function  $g(\omega)$ , and hence of the Stribeck phenomenon, near zero velocity. Its value is taken between 1 and 2, depending upon the ODE solving capability of the simulator. Since  $T_s \geq T_c$  the value of  $g(\omega)$  remains strictly positive [15].

## V. COMPLETE MODEL

Using equations (8) (9) and (10), the complete system model can be expressed in light of equation (2) as:

Let

$$\begin{aligned} x_1 &= \theta, \quad x_2 = \frac{d\theta}{dt}, \quad U = \overline{V_a} \\ \dot{x}_1 &= x_2, \quad \dot{x}_2 = -\omega_n^2 x_1 - 2\zeta\omega_n x_2 + K\omega_n^2 U \\ \text{If } X &= \begin{bmatrix} x_1 \\ x_2 \end{bmatrix} \text{ Then } \dot{X} = \begin{bmatrix} 0 & 1 \\ -\omega_n^2 & -2\zeta\omega_n \end{bmatrix} X + \begin{bmatrix} 0 \\ K\omega_n^2 \end{bmatrix} U \\ Y &= [1 \ 0] X \\ \omega_n &= \sqrt{\frac{K_{spr}}{J_{tot}}}, \quad \zeta = \frac{K_a^2(\theta)}{2R_a \sqrt{J_{tot} K_{spr}}}, \quad K = \frac{K_a(\theta)}{K_{spr} R_a} \\ T_{pc} &= \text{Const}, \quad T_f = \sigma_o z + \sigma_1 \dot{z} + \sigma_2 \omega \\ \dot{z} &= \omega - \sigma_o \frac{|\omega|}{g(\omega)} z \\ g(\omega) &= T_c + (T_s - T_c) e^{(-\omega/|\omega_s|)^\alpha} \end{aligned}$$

## VI. SYSTEM IDENTIFICATION

Figure 7 shows the typical characteristics of our modeled system in terms of the output angle with respect to the applied duty cycle. The lack of movement at the start and the hysteresis in shaft position upon change of direction is the most prominent feature of the actuator as it represents the existence of nonlinearities in the system, arising from the presence of pre-compression and friction forces.

With fig. 7 as a reference, we define  $D$  as the applied duty cycle,  $D_a$  as the duty cycle at which the actuator moves,  $D_{pc}$  as the duty-cycle leading to countering the spring pre-compression and  $D_s$  as the amount countering the static friction. The value of static friction and spring pre-compression torque can directly be calculated from the graph, once we find out  $K_a(\theta)$ . Of course, the nominal value of  $K_a(\theta)$  will be used, i.e. the value in the constant region.

$$D_s = \frac{T_s R_a}{K_a(\theta) V_s}, D_{pc} = \frac{T_{pc} R_a}{K_a(\theta) V_s}$$

The effective duty-cycle and armature voltage then become:

$$D_a = D - (D_{pc} + D_s)$$

$$\overline{V_a} = D_a V_s$$

for all positive values of  $D_a$  and 0 for the rest.

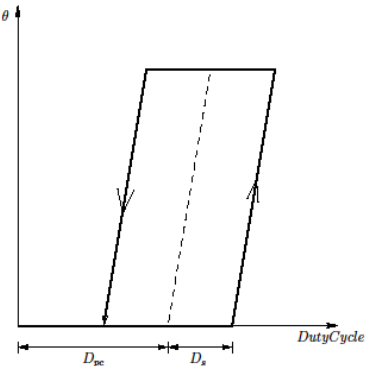


Figure 7: Characteristic Curve

### A. Motor parameter identification

Identification was based on experiments conducted on a test bench which was equipped with a dynamometer for torque measurement. First, the spring constant was identified by measuring torque at different angles without energizing the actuators. Both  $K_{spr}$  and  $T_{pc}$  were measured.  $K_a(\theta)$  was measured by locking the rotor at certain angles and measuring the torque at 1Amp current. The curves so obtained are shown in figure 8. As it can be seen, the torque is almost constant in the region between 10° and 80°. This constant value was taken as nominal value of the torque coefficient.

The resistance  $R_a$  of the actuators was calculated by measuring the voltage and current in locked rotor state. The identified parameters are given in table 1.

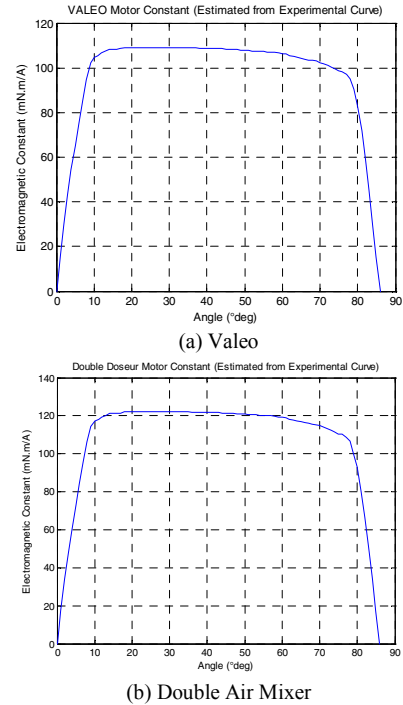


Figure 8. Variation of Motor Constant with Angle

### B. LuGre Model parameter identification

Since the spring pre-compression and nominal motor coefficient have been found out, the static friction has been identified from the characteristic curve using the relationship between duty cycle and  $T_s$  (fig. 7). This identification allows us to simplify the LuGre model by assuming  $\sigma_0 z = g(\omega)$  and  $\alpha = 1$  [17]. Also, since the actuator rotors are simply mounted on ball bearings the effect of viscous friction is minimal. Hence  $\sigma_2$  can be neglected. If we consider the system in constant velocity state then  $z$  is equal to zero. Then equation (9) can be expressed as:

$$\sigma_0 z = g(\omega) \frac{\omega}{|\omega|}$$

Considering the torque balance equation (equation(2)), if the pre-compression torque is considered a part of spring torque, then the steady state expression becomes [17]:

$$T_m + T_{spr} = \left[ T_c + (T_s - T_c) e^{(-\omega/|\omega_s|)} \right] \frac{\omega}{|\omega|}$$

This expression can be used to estimate  $\omega_s$  and  $T_c$  through non-linear least squares method.  $\sigma_0$  can be found out by curve fitting to adjust the slope of the static friction component. The most difficult parameter to identify is  $\sigma_1$ . Methods proposed for its identification involve the application of genetic algorithm [15] and blackbox identification methods such as ARX [17]. Canudas [18] has approximated  $\sigma_1$  as the square root of  $\sigma_0$  for simulation. This can be validated through experimental results of Thierry [17]. The estimated values for friction parameters are given in table 2.

## VII. PARAMETER VALIDATION

The motor-spring parameters identified through experiments are given in table 1. The identified and estimated parameters for LuGre model are given in table 2. The simulated results are displayed in the fig. 9.

Table 1: Motor-Spring Parameters

	$K_a$ mN.m/ $A$	$R_a \Omega$	$K_{spr}$ mN.m/rad	$J_{tot}$ Kg.m <sup>2</sup>	$T_{pc}$ mN.m
Valeo	109.1	3.75	45.97	1.30e-7	37.9
Delphi	120	2.79	114.28	1.68e-7	45.16

Table 2: LuGre parameters

	$T_{static}$ mN.m	$T_{coulomb}$ mN.m	$\sigma_0$	$\omega_s$ rad/sec
Valeo	12.633	12.18	28e <sup>2</sup>	1.01e <sup>-3</sup>
Delphi	12.9	12.34	31e <sup>2</sup>	1.16e <sup>-3</sup>

## VIII. CONCLUSION

The simulator values correspond to the experimental values in the envelope of a second order system. The motor electromagnetic torque constant  $K_a$  has been evaluated experimentally and used in simulation. Since in a torque motor, the torque depends upon the motor angle as well, it is important to find a mathematical model for future. However, a complete and precise model would depend upon the stator and rotor dimensions. At present a parametric model is under consideration.

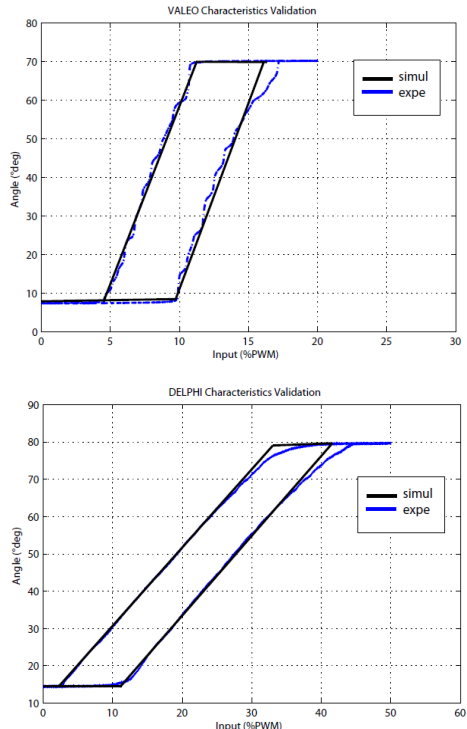


Figure 9: Simulation vs. Experiment

## REFERENCES:

- [1]. R. Hoseinnezhad, A. Bab-Hadiashar, Missing Data Compensation for Safety-Critical Components in a Drive-by-Wire System”, *IEEE Trans. Vehicular Technology Vol. 54* (July 2005)
- [2]. M. Bertoluzzo, G. Buja, J. R. Pimentel, “Design of a Safety-Critical Drive-By-Wire System Using FlexCAN” *SAE International (2005)*
- [3]. R. Isermann, R. Schwarz, S. Stolzl, “Fault-tolerant drive-by-wire systems” *Control System Magazine* 22 22-24 (2002)
- [4]. “Contactless direct drive” *Soncetboz MOVE n°5*
- [5]. M. C. Leu, R. A. Aubrecht, “Feasible and Optimal Designs of Variable Air gap Torque Motors” *Journal of Engineering for Industry, ASME* (1991)
- [6]. A. G. Mikarov, “Brushless DC torque motors quality level indexes for servo drive applications” *EUROCON'09 IEEE* (2009)
- [7]. Y. Zhang “High Performance DSP based Servo Drive Control for a Limited Angle Torque Motor” *Thesis at Loughborough University, England* (1997)
- [8]. D. Chunyang, L. Tiecai, C. Zhengcui, “Accurate Tracking Control of a Limited Angle Torque Motor” *Industry Applications Conference, IEEE* (2003)
- [9]. C. Tsai, S. Lin, H. Huang, Y. Cheng, “Design and control of a brushless DC limited-angle torque motor with its application to fuel control of small-scale gas turbine engines” *Mechatronics* 19 29-41 (2009)
- [10]. R. K. Jurgen , C. Menard, “A New Multipurpose Servo Valve for Fast Applications” *Actuators SAE* (1994)
- [11]. R. Scattolini, C. Siviero, M. Mazzucco, S. Ricci, L. Poggio and C. Rossi, “Modeling and Identification of an Electromechanical Internal Combustion Engine Throttle Body” *Control Eng. Practice* Vol. 5. No.9. pp. 1253-1259 (1997)
- [12]. H. Olsson, K.J. Åström, C. Canudas de Wit., M. Gäfvert, P. Lischinsky, “Friction Models and Friction Compensation” *European Journal of Control* 4(3) (1998)
- [13]. F. Contreras, I. P. Quiroz, C. C. deWit, “Further Results on Modeling and Identification of an Electronic Throttle Body” *Proc. 10<sup>th</sup> Mediterranean Conf. on Control and Automation-MED* (July, 2002)
- [14]. D. Karnopp, “Computer Simulation of Stick-Slip Friction in Mechanical Dynamic Systems ” *ASME Journal of Dynamic Systems, Measurement and Control, 107, 100-103* (1985)
- [15]. Z. Wenjing, “Parameter identification of Lugre Friction Model in Servo System Based on Improved Particle Swarm Optimization Algoritm”, *Proc. 26<sup>th</sup> Chinese Control Conference* 135-139 (2007)
- [16]. C. Garcia, “Comparison of friction models applied to a control valve” *Control Engineering Practice* 16 (2008)
- [17]. S. Thierry, “Modélisation et compensation du frottement dans un moteur linéaire”, *Thesis at École Polytechnique fédérale de Lausanne, France* (2005)
- [18]. C. C. de Wit, H. Olsson, k. J. Astrom, P. Lischinsky, “A new model for control of systems with friction”, *IEEE trans. Automatic control, vol. 40, No. 3* (1995)